

High-contrast imager for Complex Aperture Telescopes (HiCAT): 3. first lab results with wavefront control.

Mamadou N'Diaye^{a*}, Johan Mazoyer^a, Elodie Choquet^a, Laurent Pueyo^a,
Marshall D. Perrin^a, Sylvain Egron^{b,a}, Lucie Leboulleux^{b,a}, Olivier Levecq^{b,a},
Alexis Carlotti^a, Chris A. Long^a, Rachel Lajoie^a, and Rémi Soummer^{a†}

^a Space Telescope Science Institute, 3700 San Martin Drive, Baltimore, MD 21218, USA

^b Institut d'Optique Graduate School (Palaiseau, Saint-Etienne, Bordeaux), France

ABSTRACT

HiCAT is a high-contrast imaging testbed designed to provide complete solutions in wavefront sensing, control and starlight suppression with complex aperture telescopes. The pupil geometry of such observatories includes primary mirror segmentation, central obstruction, and spider vanes, which make the direct imaging of habitable worlds very challenging. The testbed alignment was completed in the summer of 2014, exceeding specifications with a total wavefront error of 12nm rms over a 18mm pupil. The installation of two deformable mirrors for wavefront control is to be completed in the winter of 2015. In this communication, we report on the first testbed results using a classical Lyot coronagraph. We also present the coronagraph design for HiCAT geometry, based on our recent development of Apodized Pupil Lyot Coronagraph (APLC) with shaped-pupil type optimizations. These new APLC-type solutions using two-dimensional shaped-pupil apodizer render the system quasi-insensitive to jitter and low-order aberrations, while improving the performance in terms of inner working angle, bandpass and contrast over a classical APLC.

Keywords: high angular resolution, coronagraphy, wavefront sensing, wavefront control

1. INTRODUCTION

Several space telescopes are currently investigated (e.g. WFIRST-AFTA¹ with monolithic mirror, Large Ultraviolet Optical Infrared [LUVOIR] telescopes with segmented primary mirror, such as ATLAST^{2,3} or HDST⁴) and one of their key goal is the direct imaging and spectroscopy of extrasolar planets, and possibly habitable worlds. However, their aperture geometry makes high-contrast imaging challenging, in particular on two aspects: coronagraphy for starlight suppression and wavefront calibration for contrast stability in the presence of vibrations. We are currently developing HiCAT, a STScI testbed to provide system-level solutions combining wavefront sensing, wavefront control and starlight suppression strategies on such apertures.

Within this framework, we also explore novel high-contrast strategies, including:

- novel pupil remapping techniques (e.g. Active Control of Aperture Discontinuities [ACAD]⁵) that use two deformable mirrors (DMs) to re-shape complex pupil (including struts and segment gaps) and offer friendly apertures to coronagraph systems. Recent developments are presented in a companion paper by Mazoyer et al. in these proceedings.
- innovative coronagraph designs for any type of apertures (e.g. for the Apodized Pupil Lyot Coronagraph [APLC] based on our recent developments for circular axi-symmetric pupil⁶ or complex geometry apertures⁷).

In our previous paper,⁸ we report on the design overview and the first light results of HiCAT after finalized alignment in the absence of DMs. In this communication, we present our recent developments on HiCAT with the presence of a single facesheet Boston DM and our new findings in coronagraphy for arbitrary apertures.

*E-mail: mamadou@stsci.edu, †: HiCAT bench Principal Investigator

In Section 2, we present the main features of our testbed. In Section 3, we report on the characterization of our Boston DMs and the integration of a single device in the HiCAT optical train. In Section 4, we present preliminary wavefront control results on the testbed using a single DM and a classical Lyot coronagraph. Finally in Section 5, we show our recent progress in coronagraphy for arbitrary apertures with further implementation in our testbed.

2. HICAT MAIN FEATURES

The testbed optical design was developed using an hybrid approach to define the layout and surface error requirements to minimize amplitude-induced errors, so-called Talbot effects to develop methods for aperture diffraction control. The complete details of our design study are presented in our previous communications.^{8,9} Our testbed uses mirrors with high surface quality (better than $\lambda/40$) based on our specifications that are derived from our high-contrast requirements (10^8 contrast floor inside a half-field dark hole produced by a single DM with a perfect coronagraph from 3 to 10 λ/D with 2% bandpass). The testbed design includes several features:

- a 20 mm pupil mask to mimic the central obstruction and the support struts of the telescope aperture and enable the replication of monolithic telescope geometries such as WFIRST-AFTA.
- three DMs: an Iris AO segmented mirror to mimic segmentation of the telescope primary mirror with 36 segments, similar to ATLAST/HDST, and 2 Boston kilo-DM for wavefront control and pupil remapping techniques such as ACAD.⁵
- a starlight suppression system based on the APLC¹⁰ architecture: a reflective apodizer for broadband operations based on the recent developments made by JPL and Princeton¹¹ and relying on our recent solutions,⁶ a reflective, focal plane mask (FPM) inherited from the Lyot project¹² and a motorized Lyot stop.
- two cameras (CamF and CamP) respectively for focal and pupil plane imaging are part of the back end. CamF is positioned on a translation stage to enable direct and coronagraphic phase diversity measurements.^{13,14}

The testbed also have additional room for further implementation of low- and mid-order wavefront sensing concepts such as the Zernike wavefront sensors.^{15,16} Additional feature includes the 4D Fizeau interferometer outside the main optical path for alignment purpose and direct wavefront sensing measurements.

In June 2014, the reflective apodizer and the different DMs were not available yet. They were replaced by flat mirrors with excellent surface error quality ($\sim \lambda/20$ PV surface error over a 2-inch diameter). After procurements of the optical and mechanical parts, we performed the alignment of the testbed and last summer, we obtained our first PSFs in the absence of DMs, see Figure 1. We achieved an optical quality of 12nm rms over a 18mm pupil after passing through an optical train of 15 components. At the end, this testbed will combine a segmented DM to mimic the aperture segmentation, a pupil mask for the central obstruction and spiders of the telescope, two Boston DMs for wavefront control and an APLC for starlight suppression.

3. HICAT DEFORMABLE MIRRORS

3.1 Environment control

During last winter, we received our science grade Boston kilo-DMs for wavefront control and pupil remapping applications with HiCAT. These devices must operate in a clean environment with a relative humidity that remains below 30% for long-term reliability. In particular, humidity is a critical issue since the application of voltage in humid environment leads to corrosion effects on the DM that are irreversible.^{17,18}

HiCAT is located in the STScI Makidon Optics Lab in a class 1000 clean room with a temperature that is controlled to within 1°C and relative humidity that remains below 40%. In addition to our lab humidity control, we recently installed a dry air system to our experiment. This system injects 1.5 psi pressure dry air with the

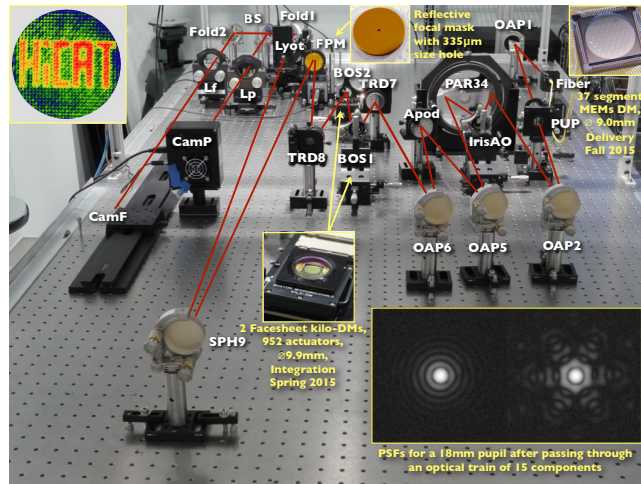


Figure 1. Overall picture of the HiCAT in June 2014. The alignment was completed in June 2014 in the absence of DMs. We obtained our first PSFs in log scale at the FPM with a 18 mm unobstructed circular aperture and a JWST-like pupil, see inset images. Seven regular diffraction rings can be observed, confirming the good quality of our alignment and of our optics.

output split between 6 lines to different points of the $\sim 4m^3$ HiCAT enclosure. With this additional system in our testbed, we keep the relative humidity below 30%. In addition, we use temperature and humidity sensors to continuously monitor the environment, ensuring the DM is used only in adequate conditions (see Figure 2).

The dry air system may add unwanted turbulence effects, leading to wavefront variations that makes high-contrast regimes stability challenging. Further plans include the installation of a second stage humidity control within the whole room to keep the humidity below 30% while minimizing the turbulence effects during experiments.

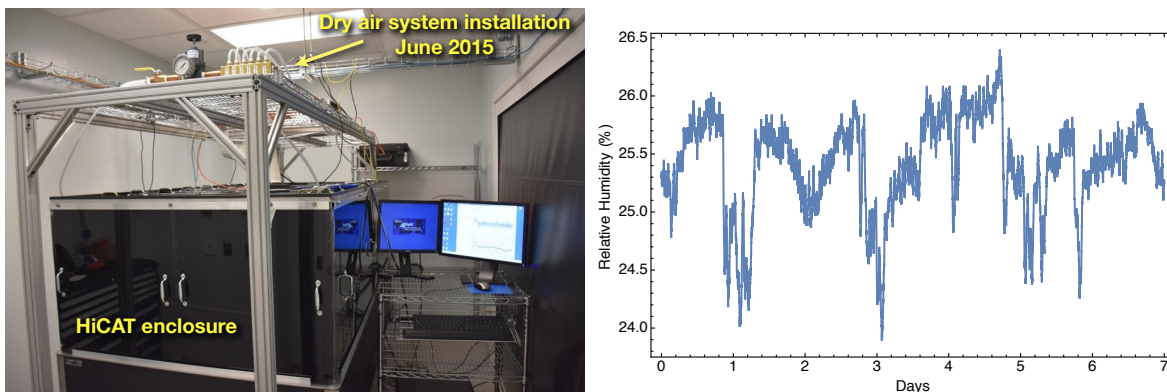


Figure 2. Environment control for the HiCAT experiment. **Left:** Picture of the testbed enclosure and its dry air system. The latter was installed in June 2015 in support to the room humidity control system to reach a relative humidity below 30%, allowing us to operate the DMs without risk of corrosion. **Right:** Relative humidity measurements obtained during the first week of August 2015, showing relative humidity values around 25%. Measurements inside the enclosure are permanently performed to monitor the relative humidity and ensure the adequate use of our DMs in the right conditions.

3.2 DM characterization

Having a good knowledge of our DM behavior is a key point for further wavefront control operations. To obtain such information, we calibrate our DMs using our 4D Fizeau interferometer in front of it. Based on previous analysis studies,^{18,19} we set all the actuators to a DM flat position using a close loop with the 4D Fizeau interferometer. We chose to set this flat position around voltages of 70% of the maximum voltage of the DM

to ensure a maximum actuator stroke range during operation. From this reference point, we apply different voltages values from -60% to 20% to every forth actuator across a row and a column. This operation allows us to avoid cross-talk when determining the influence function of each actuators and test all the actuators in just four iterations. Finally, we measure their displacement with the interferometer to determine the actuator influence function.

We retrieve a quadratic response curve representing the stroke as a function of the applied voltage for each actuator (see Figure 3, left) and determine the maximum, the minimum and the stroke range of every actuators. On Figure 3 we show for every actuator the maximum values reachable under (center) and above (right) the reference flat position. From this analysis, we deduce that in the worst case, the minimum stroke range for an actuator around the flat position is 632 nm. Mazoyer et al. (submitted)²⁰ recently made a study on the ACAD applicability on the testbed, considering an WFIRST-AFTA-like pupil, our current DMs characteristics and their separation, see Figure 4. The authors estimated a 470 nm maximum required stroke range to set up the shape of the DMs for application of the pupil remapping technique. This value is well within the measured stroke range for every actuators, confirming the possibility to validate ACAD on HiCAT in laboratory.

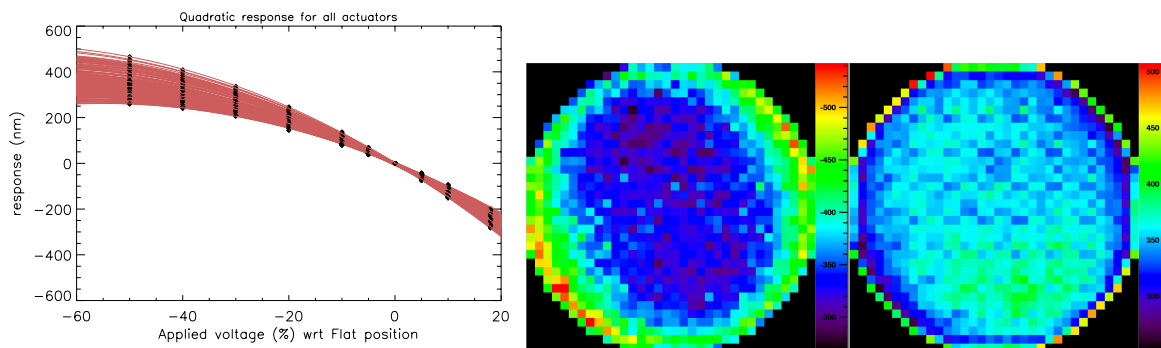


Figure 3. Characterization of our first Boston DM. **Left:** Quadratic response curves for each of the 952 actuators of our DM after interpolation of our measurements represented by black dots. For these measurements, we position the DM in front of our Fizeau interferometer, apply a flat reference of the DM (chosen around 70% of the maximum voltage), and introduce push-pull from this reference to each actuator to determine the influence function for different voltages. The 70% maximum voltage reference point was chosen to ensure a maximum stroke range for our actuators. After analysis of all our actuators, we estimate a minimum available stroke range of 632 nm. **Right:** Maps of the maximum achievable stroke under and above the flat position for each actuator. As expected, the distribution of strokes follows the chip shape of the DM at rest.

3.3 DM integration

The Boston DMs have two dedicated locations in the HiCAT optical train, the first one in a pupil plane conjugated to the pupil mask and the second one at 30 cm away from the first device in an out-of-pupil plane to perform both phase and amplitude error corrections. The science grade DMs were not available during our alignment in June 2014 and we replaced them by high-quality flat mirror ($\lambda/20$ PV surface error over a 2-inch diameter part).

After DM characterization, we removed the flat mirror present at the pupil plane location and integrated our first device in Spring 2015. After fine DM positioning, we flattened it and used our interferometer to determine the quality of our alignment. We estimated an optical quality of 13 ± 3 nm rms wavefront error over 18 mm size pupil, see Figure 5. These values with one DM inserted, with no significant loss in terms of wavefront quality, are almost equivalent to our estimates before insertion, confirming the excellent quality of our DM alignment.

We also determine a contribution below 10 nm rms for the low-order aberrations. These small WFE rms values are promising for application of wavefront control algorithms, such as Energy minimization,²¹ Electric Field Conjugation²² or Stroke minimization.²³ Before considering such algorithms and as a first step, we started our work on speckle nulling algorithms to check our system.

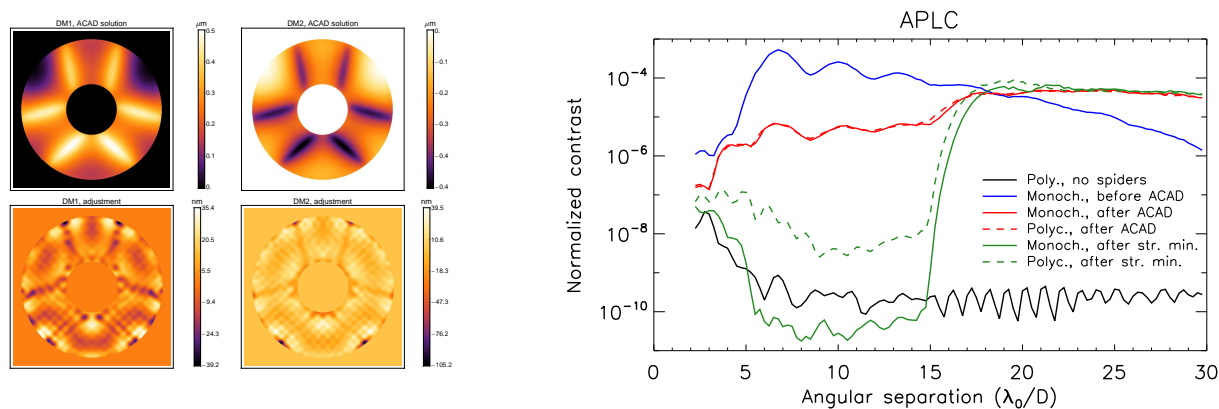


Figure 4. ACAD studies with WFIRST-AFTA like pupil in preparation for implementation in HiCAT. **Left:** DM shapes at different stages of the ACAD + stroke minimization process for an WFIRST-AFTA like pupil with the HiCAT parameters. Top: Shapes of the ACAD solution for the DM 1 and 2. The deformation strokes are inferior to 450 nm. Bottom: adjustments around this shape after the stroke minimization algorithms. These deformation strokes are inferior to 150 nm. The final strokes (ACAD + Stroke Minimization) are inferior to 470 nm. **Right:** Radial contrast profile of the images at different stages of the ACAD + stroke minimization process for an WFIRST-AFTA like pupil. These contrasts are normalized by the intensity peak of the PSF without coronagraph. Results in monochromatic and 10% broadband light are represented in solid and dashed lines. The black curve represents the contrast obtained with an APLC in polychromatic light in the case of a 36% central obscuration pupil and no struts. The blue line shows the contrast after the introduction of the WFIRST-AFTA support structures of the secondary in the pupil. In red, the contrast in the dark hole after the ACAD solution. Finally, we present the final contrast obtained after ACAD and stroke minimization correction (green curve). A dark hole contrast better than 6.10^{-11} is obtained in monochromatic light and 1.10^{-8} in broadband light on a 5-15 λ/D dark hole, showing the efficiency of our combined solution. From Mazoyer et al. (submitted).²⁰

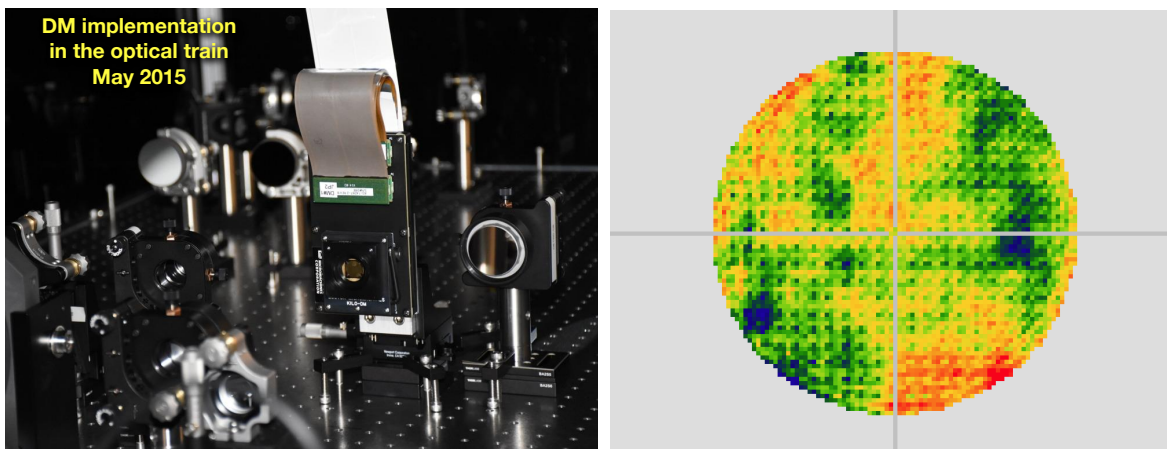


Figure 5. **Left:** Picture of the DM after integration in the optical train of the testbed. **Right:** Example of wavefront map (10.5 nm rms and 55.0 nm peak-to-valley wavefront error here) obtained after DM flattening with our Fizeau interferometer after alignment. We measured an optical quality of 13 ± 3 nm rms wavefront error after alignment and below 10 nm rms for the low-order aberrations, reaching a quality quasi-equivalent to the one we obtained before DM insertion. These small values are really promising for the direct application of fine wavefront control algorithms, such as Electric Field Conjugation^{21, 22} or Stroke Minimization.²³

4. FIRST WAVEFRONT CONTROL RESULTS

Prior to the 2015 SPIE conference, we started with the implementation of speckle nulling algorithm on HiCAT. Our testbed configuration includes a 18 mm size circular non obstructed pupil, a single Boston DM, a classical Lyot Coronagraph with 335 μm size reflective FPM (5.91 λ_0/D relative size for a F/89 beam at $\lambda_0 = 638$ nm)

and a 10 mm diameter Lyot stop.

We first perform the calibration aspects with our DM in flat position by acquiring coronagraphic images onto CamF. Their analysis allows us to retrieve the plate scale, the optical axis position, the DM orientation and the contrast.

After calibration, we select one speckle and determine the corresponding spatial frequency of the sine wave pattern. We then probe for the speckle phase by first acquiring four images with this sine pattern on the flattened DM with phase shifts of respectively 0 , $\pi/2$, π , $3\pi/2$. We estimate the speckle intensity for each image to interpolate a sine wave function and we derive the phase shift for the sine wave pattern on the flattened DM that minimizes the speckle intensity. We then determine the speckle amplitude based on its relation with the speckle normalized intensity in the initial image.

We finally combine the flat position with the estimated sine wave pattern on the DM to attenuate the considered speckle. Figure 6 shows the images before and after DM shaping, showing our first single speckle nulling. The fact that the targeted speckle (circled in white) and its symmetric with respect to the main optical axis (circled in blue) are corrected simultaneously underlines the prevalence of phase errors over amplitude errors at these contrast levels and in that specific image location. This wavefront control step is a preliminary result which paves the way for multi-speckle nulling over a one-side dark hole.

However, we do not expect high contrast level in this configuration since we are equipped with a classical Lyot coronagraph. In this context and in view of the future exoplanet direct imaging missions with arbitrary apertures, we have been developing novel designs to push starlight suppression further.

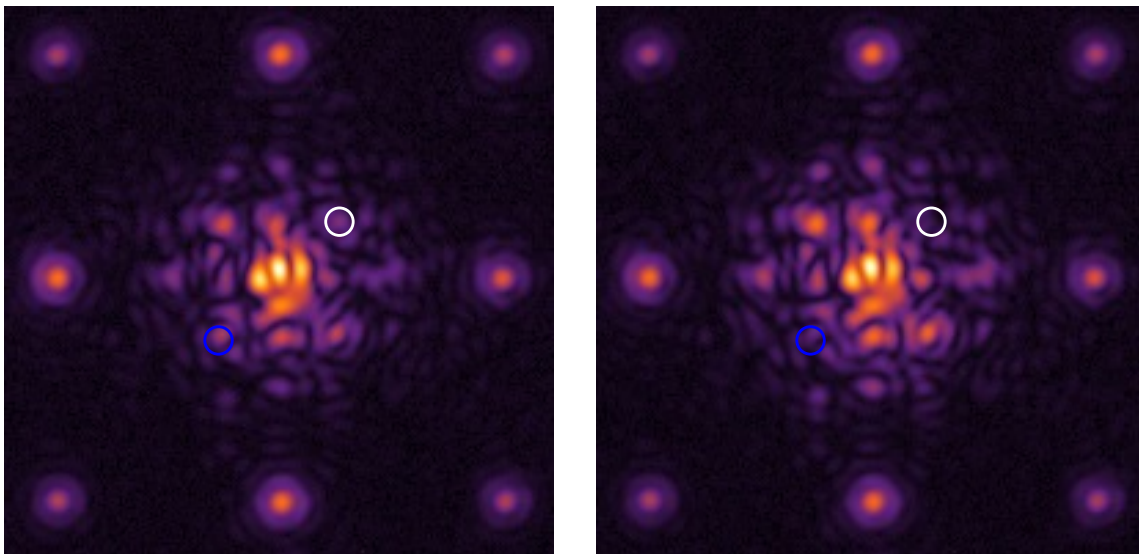


Figure 6. Coronagraphic images before and after nulling of a single speckle denoted by the white circle. The blue circle represents the symmetric location of the considered speckle with respect to the main optical axis. Light attenuation is observed in both locations, suggesting the domination, at these contrast levels, of phase errors over amplitude errors in HiCAT as we expected when we start the testbed design. Further studies with speckle nulling over a given dark zone will allow us to verify this important aspect for further high-contrast studies with unfriendly apertures.

5. NOVEL CORONAGRAPH DESIGNS

Coronagraphs design for 10^{10} contrast performance with large segmented aperture is one of the key issue for the direct imaging and spectroscopy of habitable worlds with future large missions. Several approaches have been studied over the past few months to overcome this issue. Our approach addresses the Apodized Pupil Lyot Coronagraph (APLC), a diffraction suppression system that is currently implemented in the recently deployed exoplanet direct imagers P1640, GPI and SPHERE.

The APLC combines a classical Lyot coronagraph with entrance pupil apodization to achieve starlight suppression.^{24,25} For these instruments, the apodization uses a prolate function which is an eigenfunction of the Lyot-style coronagraphic propagation problem for a given mask size. The designs have been optimized considering the contrast as a metric and exploring the parameter space with these prolate functions and the Lyot stop geometry. These solutions are quasi-achromatic and provides a theoretical contrast of 10^7 at $0.2''$ in H-band.^{10,26} However, these designs are limited in terms of contrast and IWA.

In this context, we have considered another method to derive novel solutions. This approach is based on shaped pupil type optimization which consists of finding apodizations to produce PSF dark zones. With this method, we increase the number of degrees of freedom with respect to the eigenvalue problem approach: we set the contrast, IWA, bandpass and Lyot stop geometry and we seek for the apodization with the highest throughput that solves the problem.

5.1 Circular axi-symmetric pupils

As a first step, we considered circular axi-symmetric pupils and we found novel solutions that were introduced in N'Diaye et al.⁶ In the context of GPI, we showed our ability to gain one order of magnitude in terms of contrast and $1 \lambda/D$ in IWA.⁶

More interestingly, we showed the existence of solutions which produces PSF core smaller than the projected coronagraphic mask. This allows PSF movement within the mask with no impact on the coronagraph performance. Our new concepts are therefore more robust to tip, tilts, focus drifts and other vibrations, a major concern in coronagraphy.

In the context of GPI, we show that our new designs offer a better contrast and a lower sensitivity to low-order aberrations. We also provide 10^{10} contrast designs with an IWA that depends on the bandpass and the central obstruction size, see N'Diaye et al. for further details.⁶

5.2 Arbitrary apertures

5.2.1 Solution for large segmented aperture

These proposed solutions essentially apply to circular axi-symmetric apertures, corresponding to a one dimension radial problem. The presence of spiders struts and segment gaps in the pupil will alter the coronagraph performance. This effect can be mitigated with the use of ACAD solutions⁵ upstream the diffraction suppression system.

An alternative, complementary approach consists of developing coronagraphic solutions that work with unfriendly pupils. Both Princeton University and STScI teams recently develop novel approaches in the context of WFIRST-AFTA and ATLAST based on APLC and shaped pupil coronagraphs. These approaches extend our previous method for one-dimension radial problem to two-dimension problem. The Princeton team develops the Shaped pupil approach and combines it with a classical Lyot coronagraph to increase the coronagraph performance. At STScI, we consider the APLC and look for apodizers with Shaped pupil solutions. These close paths were studied in parallel in the context of WFIRST by Princeton and in the context of segmented apertures by STScI.

We consider the telescope and coronagraph parameters given in Table 1 and following our developed approach, we recently found solutions with APLC using a shaped pupil that provides a 10^{10} contrast PSF dark zone over a 10% bandpass, with a moderate inner working angle, see Figure 8.

5.2.2 Apodizer manufacturing aspects

Our solution uses an 600-point diameter across apodization that is not fully binary. Increasing the number of points results in a heavy computational problems that cannot be resolved with our current resources. We consider another approach starting from our current numerical solution. We first test a design with rounded values of our numerical solution. This leads to a contrast loss of two orders of magnitude.

To recover the ultimate 10^{10} contrast, we use an binary approximation which combines a sub-pixelisation of the current solution points and the error diffusion algorithm.²⁷ With a 16 factor pixelization, we achieved a binary design that almost provides a 10^{10} contrast, see Figure 7.

Based on current technologies for the fabrication of a reflective apodizer, we assume a black silicon pattern mask with $15\ \mu\text{m}$ size pixel. A binary mask for our design is feasible with a 144 mm diameter prototype. This is a very encouraging result since our design is manufacturable as-of-today with current technologies and further improvements on size reduction or design are expected to reduce the prototype size.

This concept is furthermore robust to low-order aberrations, providing room for small vibrations of the instrument. Working with large telescope however leads to observation of resolved stars and stellar angular size is a major concern in coronagraphy.²⁸

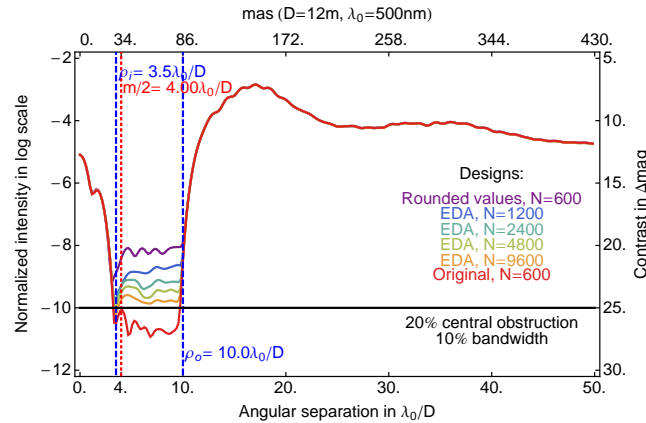


Figure 7. Azimuth averaged intensity profile of the coronagraphic image reached by an APLC solution in 10% broadband light and the parameters shown in Table 1, except for the Lyot stop which presents a 36% instead of 40% obstruction, providing a quasi-binary shaped pupil. Profiles are represented for the design with the original grey version, rounded values version, and the binarized versions using error diffusion algorithm (EDA, see e.g.²⁷) with different lateral size N obtained by sub-pixelization of the original design gray pixels. The dashed blue vertical lines delimit the high-contrast search area \mathcal{D} ($\rho_i = 3.5\lambda_0/D$ and $\rho_o = 10.0\lambda_0/D$). The red dot line delimits the FPM radius, set to $m/2 = 4\lambda_0/D$. The averaged contrast over the spectral band in the dark region is below 10^{-10} (black horizontal line). The 10^{10} contrast performance of the original design is almost recovered with a EDA version using $N=9600$. Relating on current black silicon technologies to manufacture Shaped pupil mask for WFIRST-AFTA coronagraph,¹¹ we translate these values into physical units. Assuming a $15\ \mu\text{m}$ size for a pixel, the apodizer of our design can currently be fabricated with a 144 mm diameter prototype to work in visible light.

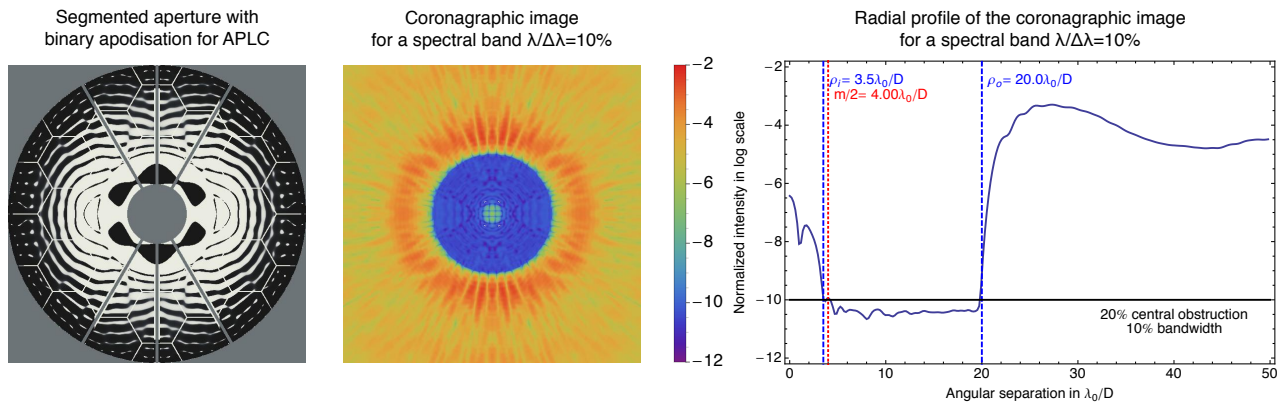


Figure 8. **Left:** Shaped pupil apodization for the APLC coronagraph for the ATLAST mission. **Middle:** Coronagraphic image obtained with the coronagraph for a 10% spectral bandwidth. A dark zone with a 10^{10} contrast level is produced with the segmented aperture, paving the way for the observation of habitable worlds. **Right:** Radial intensity profile of the previous image with the size of the focal plane mask and the dimensions of the high-contrast region delimited in red and blue. The stellar image core is smaller than the mask, allowing an enlargement or a displacement within the mask without impact on the contrast zone, making the design virtually insensitive to low-order aberrations, such as pointing errors or defocus drifts.⁷

Table 1. Parameters for the design showed in Figure 8.

parameters	value
Contrast C	10
Dark zone inner edge radius ρ_i	$3.5 \lambda_0/D$
Dark zone outer edge radius ρ_o	$20.0 \lambda_0/D$
focal plane mask radius $m/2$	$4.0 \lambda_0/D$
Aperture	20% central obstruction 1% aperure size spiders 0.2% aperture size gaps
Lyot stop	40% central obstruction 2% aperutre size spiders no segmentation
Broadband optimization	3 wavelengths within 10% band

5.2.3 Sensitivity to stellar angular size

We study the impact of stellar leaks on our concept due to stellar angular size. Figure 9 show the contrast at $5 \lambda_0/D$ as a function of the stellar angular size for a 12m telescope at 500nm. We can notice a plateau on the contrast curve, showing the stability of our concept to resolved stars. Actually, our concept can observe a Sun-like star beyond 4.4pc with a 12m telescope without being impacted by the stellar angular size, proving very encouraging for future direct imaging space missions.

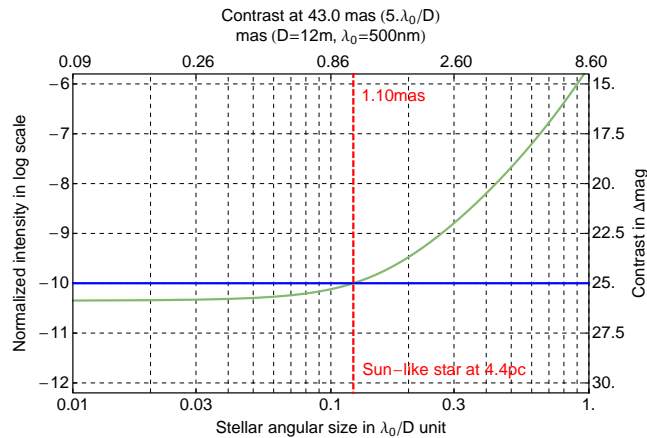


Figure 9. Averaged intensity of the broadband coronagraphic image at a $5 \lambda_0/D$ angular separation from the optical axis as a function of the stellar angular size. The curve is obtained for our design with $\rho_1 = 20 \lambda_0/D$. Blue solid line denotes the 10^{-10} intensity level. Our design presents a plateau and intensity levels below 10^{-10} for stellar angular size up to $0.12 \lambda_0/D$, underlining the contrast performance stability of our coronagraph design. Assuming a 12m telescope at 500 nm, our coronagraph is robust to stellar angular sizes up to 1.1 mas, allowing observations of planets around Sun-like star located beyond 4.3 pc.

Following these results, we decide to simulate the image of a solar system twin with our concept. We use a model based on spectral and spatial information from Haystack project and based on these assumptions, we produce the image in Figure 10 in which an Earth-like planet can be observed and characterize after 40h exposure time.

6. CONCLUSIONS

HiCAT is an operating testbed that enables on-axis monolithic or segmented aperture coronagraph system-level studies. The STScI facility will allow us to develop integrated solutions for unfriendly geometry aperture such

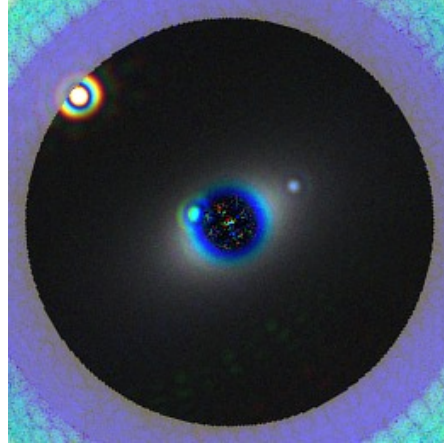


Figure 10. Simulated multicolor pictures of a solar system twin at 13.5 pc with a 12 m telescope and our coronagraph design with an OWA $\rho_1 = 30 \lambda_0/D$ at different exposure times (40h). The solar system was modeled with the Haystacks project (See A. Roberge et al., <http://asd.gsfc.nasa.gov/projects/haystacks/haystacks.html>), including spectroscopic and spatial information for all the components within the exoplanetary system. Each picture is a composite of three images on three channels around 400, 500 and 600 nm, each with 10% bandpass and a coronagraph optimized for this band. In this simulation, we assume a perfect wavefront, no wavefront drifts between the target "solar system" star and calibrator star for the image processing, and only photon noise. Earth is at 2 o'clock and is indeed blue, Venus is at 9 o'clock, Zodiacal light is elongated along the 2-8 o'clock direction, Jupiter is at 10 o'clock in the red channel (600 nm): it is outside of the dark hole at shorter wavelengths. In that channel, most of Venus is hidden by the coronagraph. Linear and logarithmic scale representations are used inside and outside the high-contrast region for each coronagraph.

as WFIRST-AFTA or HDST. To perform such studies, our testbed will rely on novel diffraction control and wavefront control schemes with multiple DMs (one segmented Iris AO and 2 Boston Micromachines).

This year, we went from the aligned testbed without DMs to preliminary results in wavefront control on testbed with one integrated DM. Our studies include the characterization of Boston DM, its integration in the HiCAT optical train, and the first single speckle nulling with classical Lyot coronagraph.

We have also explored novel coronagraph designs for arbitrary telescope apertures with further implementation in the HiCAT testbed for lab validation. We found designs that provide a 10^{10} contrast at $4 \lambda_0/D$ with moderate 18% Airy throughput for a large segmented aperture with our hybrid APLC/Shaped Pupil solution, representing a first proof of existence. Our solutions prove quasi-insensitive to low-order aberrations and stellar angular size. In addition, these solutions are manufacturable with as-of-today technologies and are fully functioning.

Our next steps includes the generation of a one side dark hole using speckle nulling algorithm during fall. We will then consider the introduction of the second Boston DM for application of ACAD in laboratory. Based on our recent studies, we will design apodizer prototypes for starlight suppression with different aperture geometries. In the long term, we will have three DMs and we will set novel system level solutions including diffraction suppression and wavefront control for high-contrast generation and stability with arbitrary apertures, advancing technologies for direct imaging and spectroscopy of habitable worlds with future space missions.

ACKNOWLEDGMENTS

This work is supported by the National Aeronautics and Space Administration under Grants NNX12AG05G and NNX14AD33G issued through the Astrophysics Research and Analysis (APRA) program (PI: R. Soummer). This material is also partially based upon work carried out under subcontract 1496556 with the Jet Propulsion Laboratory funded by NASA and administered by the California Institute of Technology. The authors warmly acknowledge Tyler Groff, N. Jeremy Kasdin, Charles-Philippe Lajoie, Bruce Macintosh, Dimitri Mawet, Colin Norman, J. K. Wallace, and Stuart Shaklan for fruitful discussions during the testbed design. The authors are also very grateful to STScI and its staff members, in particular Bill Franz, Joe Hunkeler and Kelly Coleman, for their invaluable support.

REFERENCES

1. D. Spergel, N. Gehrels, C. Baltay, D. Bennett, J. Breckinridge, M. Donahue, A. Dressler, B. S. Gaudi, T. Greene, O. Guyon, C. Hirata, J. Kalirai, N. J. Kasdin, B. Macintosh, W. Moos, S. Perlmutter, M. Postman, B. Rauscher, J. Rhodes, Y. Wang, D. Weinberg, D. Benford, M. Hudson, W.-S. Jeong, Y. Mellier, W. Traub, T. Yamada, P. Capak, J. Colbert, D. Masters, M. Penny, D. Savransky, D. Stern, N. Zimmerman, R. Barry, L. Bartusek, K. Carpenter, E. Cheng, D. Content, F. Dekens, R. Demers, K. Grady, C. Jackson, G. Kuan, J. Kruk, M. Melton, B. Nemati, B. Parvin, I. Poberezhskiy, C. Peddie, J. Ruffa, J. K. Wallace, A. Whipple, E. Wollack, and F. Zhao, "Wide-Field Infrared Survey Telescope-Astrophysics Focused Telescope Assets WFIRST-AFTA 2015 Report," *ArXiv e-prints*, Mar. 2015.
2. M. Postman, T. Brown, K. Sembach, M. Giavalisco, W. Traub, K. Stapelfeldt, D. Calzetti, W. Oegerle, R. Michael Rich, H. Phillip Stahl, J. Tumlinson, M. Mountain, R. Soummer, and T. Hyde, "Advanced Technology Large-Aperture Space Telescope: science drivers and technology developments," *Optical Engineering* **51**, p. 011007, Jan. 2012.
3. L. D. Feinberg, A. Jones, G. Mosier, N. Rioux, D. Redding, and M. Kienlen, "A cost-effective and serviceable ATLAST 9.2m telescope architecture," in *Society of Photo-Optical Instrumentation Engineers (SPIE) Conference Series*, **9143**, p. 16, Aug. 2014.
4. J. Dalcanton, S. Seager, S. Aigrain, S. Battel, N. Brandt, C. Conroy, L. Feinberg, S. Gezari, O. Guyon, W. Harris, C. Hirata, J. Mather, M. Postman, D. Redding, D. Schiminovich, H. P. Stahl, and J. Tumlinson, "From Cosmic Birth to Living Earths: The Future of UVOIR Space Astronomy," *ArXiv e-prints*, July 2015.
5. L. Pueyo and C. Norman, "High-contrast Imaging with an Arbitrary Aperture: Active Compensation of Aperture Discontinuities," *Astrophysical Journal* **769**, p. 102, June 2013.
6. M. N'Diaye, L. Pueyo, and R. Soummer, "Apodized Pupil Lyot Coronagraphs for Arbitrary Apertures. IV. Reduced Inner Working Angle and Increased Robustness to Low-order Aberrations," *Astrophysical Journal* **799**, p. 225, Feb. 2015.
7. M. N'Diaye, E. Choquet, A. Carlotti, L. Pueyo, S. Egron, L. Leboulleux, O. Levecq, M. D. Perrin, J. K. Wallace, C. Long, R. Lajoie, C.-P. Lajoie, A. J. Eldorado Riggs, N. T. Zimmerman, T. D. Groff, N. J. Kasdin, R. J. Vanderbei, D. Mawet, B. Macintosh, S. Shaklan, and R. Soummer, "High-contrast imager for Complex Aperture Telescopes (HiCAT): APLC/shaped-pupil hybrid coronagraph designs," in *American Astronomical Society Meeting Abstracts*, **225**, p. 258.09, Jan. 2015.
8. M. N'Diaye, E. Choquet, S. Egron, L. Pueyo, L. Leboulleux, O. Levecq, M. D. Perrin, E. Elliot, J. K. Wallace, E. Hugot, M. Marcos, M. Ferrari, C. A. Long, R. Anderson, A. DiFelice, and R. Soummer, "High-contrast Imager for Complex Aperture Telescopes (HiCAT): II. Design overview and first light results," in *SPIE*, **9143**, p. 27, Aug. 2014.
9. M. N'Diaye, E. Choquet, L. Pueyo, E. Elliot, M. Perrin, J. Wallace, T. Groff, A. Carlotti, D. Mawet, M. Sheckells, S. Shaklan, B. Macintosh, N. J. Kasdin, and R. Soummer, "High-contrast imager for Complex Aperture Telescopes (HiCAT): 1. Testbed design," in *SPIE*, **8864**, Sept. 2013.
10. R. Soummer, "Apodized Pupil Lyot Coronagraphs for Arbitrary Telescope Apertures," *Astrophysical Journal, Letters* **618**, pp. L161–L164, Jan. 2005.
11. K. Balasubramanian, D. Wilson, V. White, R. Muller, M. Dickie, K. Yee, R. Ruiz, S. Shaklan, E. Cady, B. Kern, R. Belikov, O. Guyon, and N. J. Kasdin, "High contrast internal and external coronagraph masks produced by various techniques," in *Society of Photo-Optical Instrumentation Engineers (SPIE) Conference Series*, **8864**, p. 1, Sept. 2013.
12. B. R. Oppenheimer, A. P. Digby, L. Newburgh, D. Brenner, M. Shara, J. Mey, C. Mandeville, R. B. Makidon, A. Sivaramakrishnan, R. Soummer, J. R. Graham, P. Kalas, M. D. Perrin, L. C. Roberts, Jr., J. R. Kuhn, K. Whitman, and J. P. Lloyd, "The Lyot project: toward exoplanet imaging and spectroscopy," in *Advancements in Adaptive Optics. Edited by Domenico B. Calia, Brent L. Ellerbroek, and Roberto Ragazzoni. Proceedings of the SPIE, Volume 5490, pp. 433-442 (2004).*, D. Bonaccini Calia, B. L. Ellerbroek, and R. Ragazzoni, eds., *Presented at the Society of Photo-Optical Instrumentation Engineers (SPIE) Conference* **5490**, pp. 433–442, Oct. 2004.

13. B. H. Dean and C. W. Bowers, "Diversity selection for phase-diverse phase retrieval," *Journal of the Optical Society of America A* **20**, pp. 1490–1504, Aug. 2003.
14. J.-F. Sauvage, L. Mugnier, B. Paul, and R. Villedieu, "Coronagraphic phase diversity: a simple focal plane sensor for high-contrast imaging," *Optics Letters* **37**, p. 4808, Dec. 2012.
15. J. K. Wallace, S. Rao, R. M. Jensen-Clem, and G. Serabyn, "Phase-shifting Zernike interferometer wavefront sensor," in *Society of Photo-Optical Instrumentation Engineers (SPIE) Conference Series*, **8126**, Sept. 2011.
16. M. N'Diaye, K. Dohlen, T. Fusco, and B. Paul, "Calibration of quasi-static aberrations in exoplanet direct-imaging instruments with a Zernike phase-mask sensor," *Astron. & Astrophys.* **555**, p. A94, July 2013.
17. H. R. Shea, A. Gasparyan, H. B. Chan, S. Arney, R. E. Frahm, D. López, S. Jin, and R. P. McConnell, "Effects of electrical leakage currents on mems reliability and performance," *Device and Materials Reliability, IEEE Transactions on* **4**(2), pp. 198–207, 2004.
18. K. M. Morzinski, A. P. Norton, J. W. Evans, L. Reza, S. A. Severson, D. Dillon, M. Reinig, D. T. Gavel, S. Cornelissen, B. A. Macintosh, and C. E. Max, "MEMS practice: from the lab to the telescope," in *Society of Photo-Optical Instrumentation Engineers (SPIE) Conference Series*, **8253**, p. 4, Mar. 2012.
19. J. Mazoyer, R. Galicher, P. Baudoz, P. Lanzoni, F. Zamkotsian, and G. Rousset, "Deformable mirror interferometric analysis for the direct imagery of exoplanets," in *Society of Photo-Optical Instrumentation Engineers (SPIE) Conference Series*, 2014.
20. J. Mazoyer, P. Pueyo, C. Norman, M. N'Diaye, R. P. van der Marel, and R. Soummer, "Active compensation of aperture discontinuities for WFIRST-AFTA: analytical and numerical comparison of propagation methods and preliminary results with an AFTA like pupil.," *subm. in JATIS* .
21. P. J. Bordé and W. A. Traub, "High-Contrast Imaging from Space: Speckle Nulling in a Low-Aberration Regime," *Astrophysical Journal* **638**, pp. 488–498, Feb. 2006.
22. A. Give'on, B. Kern, S. Shaklan, D. C. Moody, and L. Pueyo, "Broadband wavefront correction algorithm for high-contrast imaging systems," in *Society of Photo-Optical Instrumentation Engineers (SPIE) Conference Series*, **6691**, p. 0, Sept. 2007.
23. L. Pueyo, J. Kay, N. J. Kasdin, T. Groff, M. McElwain, A. Give'on, and R. Belikov, "Optimal dark hole generation via two deformable mirrors with stroke minimization," *Appl. Opt.* **48**, pp. 6296–6312, Nov 2009.
24. C. Aime, R. Soummer, and A. Ferrari, "Total coronagraphic extinction of rectangular apertures using linear prolate apodizations," *Astron. & Astrophys.* **389**, pp. 334–344, July 2002.
25. R. Soummer, C. Aime, and P. E. Falloon, "Stellar coronagraphy with prolate apodized circular apertures," *Astron. & Astrophys.* **397**, pp. 1161–1172, Jan. 2003.
26. R. Soummer, A. Sivaramakrishnan, L. Pueyo, B. Macintosh, and B. R. Oppenheimer, "Apodized Pupil Lyot Coronagraphs for Arbitrary Apertures. III. Quasi-achromatic Solutions," *Astrophysical Journal* **729**, pp. 144–+, Mar. 2011.
27. C. Dorrer and J. D. Zuegel, "Design and analysis of binary beam shapers using error diffusion," *Journal of the Optical Society of America B Optical Physics* **24**, pp. 1268–1275, June 2007.
28. O. Guyon, E. A. Pluzhnik, M. J. Kuchner, B. Collins, and S. T. Ridgway, "Theoretical Limits on Extrasolar Terrestrial Planet Detection with Coronagraphs," *Astrophysical Journal, Supplement* **167**, pp. 81–99, Nov. 2006.